remote sensing

MDPI

Article

Do Daily and Seasonal Trends in Leaf Solar Induced Fluorescence Reflect Changes in Photosynthesis, Growth or Light Exposure?

Rhys Wyber [1,*], Zbyněk Malenovský [1,2], Michael B. Ashcroft [1], Barry Osmond [1] and Sharon A. Robinson [1]

[1] Centre for Sustainable Ecosystem Solutions, School of Biological Sciences, University of Wollongong, Wollongong 2522, Australia; zbynek.malenovsky@gmail.com (Z.M.); Ashcroft@uow.edu.au (M.B.A.); cosmond@uow.edu.au (B.O.); Sharonr@uow.edu.au (S.A.R.)

[2] Department of Remote Sensing, Global Change Research Institute CAS, Bělidla 986/4a, CZ-60300 Brno, Czech Republic

* Correspondence: rawyber@gmail.com; Tel.: +61-4-3054-6291

Academic Editors: Jose Moreno and Prasad S. Thenkabail
Received: 30 March 2017; Accepted: 11 June 2017; Published: 14 June 2017

Abstract: Solar induced chlorophyll fluorescence (SIF) emissions of photosynthetically active plants retrieved from space-borne observations have been used to improve models of global primary productivity. However, the relationship between SIF and photosynthesis in diurnal and seasonal cycles is still not fully understood, especially at large spatial scales, where direct measurements of photosynthesis are unfeasible. Motivated by up-scaling potential, this study examined the diurnal and seasonal relationship between SIF and photosynthetic parameters measured at the level of individual leaves. We monitored SIF in two plant species, avocado (*Persea Americana*) and orange jasmine (*Murraya paniculatta*), throughout 18 diurnal cycles during the Southern Hemisphere spring, summer and autumn, and compared them with simultaneous measurements of photosynthetic yields, and leaf and global irradiances. Results showed that at seasonal time scales SIF is principally correlated with changes in leaf irradiance, electron transport rates (ETR) and constitutive heat dissipation (YNO; $p < 0.001$). Multiple regression models of correlations between photosynthetic parameters and SIF at diurnal time scales identified leaf irradiance as the principle predictor of SIF ($p < 0.001$). Previous studies have identified correlations between photosynthetic yields, ETR and SIF at larger spatial scales, where heterogeneous canopy architecture and landscape spatial patterns influence the spectral and photosynthetic measurements. Although this study found a significant correlation between leaf-measured YNO and SIF, future dedicated up-scaling experiments are required to elucidate if these observations are also found at larger spatial scales.

Keywords: light induced fluorescence transient; photosynthetic yield; photosynthetic active radiation; remote sensing of vegetation; pulse amplitude modulation

1. Introduction

Human driven climate change has the potential to negatively affect the growth of plants and lead to a subsequent decrease in food and fibre production [1]. Precision agriculture and plant phenotyping may increase crop yields by improving resource management and selectively breeding high yielding plants through systematic large-scale measurements of photosynthetic performance [2]. Leaf-level photosynthetic measurements have traditionally been conducted with active chlorophyll fluorescence-based approaches, such as the pulse amplitude modulation (PAM) method. While the PAM approach is a quick and well established method [3], the saturating light pulse makes it unfeasible

for measurements at the large spatial scales required for precision agriculture and plant phenotyping [4]. In recent years, the focus has shifted to the detection of solar induced fluorescence (SIF), which has shown strong potential as a photosynthesis indicator across spatial scales ranging from the leaf and canopy [5–8] to global scales [9–12].

Solar induced chlorophyll fluorescence is a broad-band-red and far-red photon emission from excited chlorophyll (Chl) molecules [13]. Changes in the level of SIF vary in proportion to the amount of absorbed photosynthetically active radiation (APAR) utilized by photochemical processes or dissipated via non-photochemical quenching (NPQ) [14]. However, in order to extract biologically relevant information from the SIF signal, information about the relative proportions of APAR used for photochemistry and NPQ must be known [14]. At large spatial scales, measurements of optical vegetation indices have been used to approximate NPQ and photochemistry. For instance, the photochemical reflectance index (PRI), which responds to changes in violaxanthin pigment de-epoxidation status (DEPS) [15], has potential to approximate information about NPQ. When combined with information from greenness optical indices, such as the normalized difference vegetation index (NDVI) [16], photosynthesis and consequently gross primary production (GPP) can be modelled at global scales [10,14,17–19]. However, how these spectral indices are related to photochemistry, NPQ and SIF cannot be examined at large spatial scales because direct measurements of photochemistry and NPQ are unfeasible. Therefore, leaf-level experiments combining spectral and active fluorescence measurements are needed.

At the leaf and small plant scale, it is possible to determine the relative proportions of energy utilized by photochemistry (YPSII/ϕPSII; for the yield of photosystem II), NPQ (YNPQ) and lost due to constitutive processes (YNO) using active fluorescence approaches, e.g., PAM [20]. By combining active fluorescence with sub-nanometre reflected radiance measurements, the relative APAR partitioning can be examined in relation to SIF, PRI and NDVI. Some studies have observed coincident changes in far-red SIF (SIF_{FR}) and ϕPSII measured by PAM fluorometers [21] and have examined diurnal and seasonal changes in SIF in crop plants [8]. However, these studies focused only on small-scale canopies in comparison with single leaf PAM measurements. The mismatch between leaf and canopy scales, results in poor correlations between leaf PAM measurements and changes in PAR measured at the canopy [8]. Moreover, to the authors' knowledge, no study has derived APAR partitioning from PAM data (i.e., YPSII, YNPQ and YNO). Instead, a leaf-level investigation which combines high frequency, daily active fluorescence measurements with sub-nanometre reflected radiance observations with the same field of view, may provide information about relationships between SIF and APAR partitioning. If such measurements are then performed over multiple seasons for multiple plant species, the generalized diurnal and season changes in SIF–APAR relationships could be examined.

In this study we aim to address the limitations of previous experiments by examining the relationships between APAR partitioning (YPSII, YNPQ and YNO) and SIF, PRI and NDVI at the leaf-level, over both diurnal and seasonal cycles. We also aim to identify the consistent relationships that hold across the examined plant species.

2. Materials and Methods

2.1. Plant Material

Measurements were performed on fully expanded leaves of two C3 plants with morphologically different foliage, avocado (*Persea americana* Mill. cv. Haas) and orange jasmine (*Murraya paniculatta* Jack). Avocado plants were grown at either the University of Wollongong, Ecology Research Centre (UOW), New South Wales (NSW), Australia (34°24′17.5″S, 150°52′17.8″E) or at Summerland House Farm (SHF), NSW, Australia (28°51′28.2″S, 153°26′24.6″E; n = 6; max PAR ~2000 µmol photons·m^{-2}·s^{-1}). Avocado plants at UOW were maintained under shade cloth (max PAR ~600 µmol photons·m^{-2}·s^{-1}; n = 3) or under full sun irradiation on a concrete slab (max PAR ~2000 µmol photons·m^{-2}·s^{-1}; n = 3). Orange jasmine plants (n = 40) were grown under full sun irradiation as

described for avocado prior to measurements (March, April, May and September). All UOW plants were grown for three months prior to measurement (April and September 2015). Well-established (~15 years) avocado trees located at SHF were grown in natural irradiation conditions (full sun) and measured in November 2015.

2.2. Fluorescence Measurements and Instrument Description

Active chlorophyll fluorescence measurements were performed using a commercially available Light Induced Fluorescence Transient instrument (LIFT) (Soliense Inc, Shoreham, NY, USA; http://www.soliense.com/LIFT_Terrestrial.php). The LIFT instrument delivers high intensity blue LED light (470 nm) to the leaf surface at a distance of up to 5 m in sequences of rapid flashlets. In a typical LIFT excitation protocol, up to 300 flashlets are delivered at high duty cycle (SQ_A phase), resulting in a gradual saturation of the observed fluorescence yield, roughly proportional to the increasing level of Q_A reduction. The next 90–120 flashlets are delivered at exponentially decreasing duty cycle (RQ_A phase), where the fluorescence yield relaxes, with kinetics defined by the rates of photosynthetic electron transport [22]. The entire fluorescence transient is then fitted using the fast repetition rate (FRR) model to determine maximum (Fm in dark or F'm in the light) and minimum fluorescence (Fo in dark or F' in the light) [23]. To ensure comparability with PAM, a cross-comparison of LIFT and PAM (miniPAM; Walz, Effeltrich, Germany) measurements was performed on avocado leaves (n = 6) during light response curves. White light at the surface of avocado leaves was modulated from 0 to 1000 µmol photons·m^{-2}·s^{-1} in 50 µmol increments, with LIFT and PAM measurements performed in replicate (n = 3) on adjacent leaf sections for each light intensity. To prevent cross interference from the PAM and LIFT flashes, measurements were offset by ~30 s and all but the adjacent measurement spots (~5 cm apart) masked by non-transmissible black cardboard. Cross-comparison of both LIFT and PAM showed YPSII measurements to be linearly related (R^2 = 0.90) and highly comparable (see supplementary material; Figure S1). For measurements of reflected leaf radiance, a QE Pro spectroradiometer (spectral range of 440 to 870 nm and spectral resolution of 0.7 nm; Ocean Optics, Dunedin, FL, USA) was mounted to the side of the LIFT instrument and optically connected via a 1 m long 400 µm optical fibre. A beam splitter was installed at the optical axis of the LIFT instrument optical path to divert 20% of the incoming radiance to the QE Pro spectroradiometer, with the remainder directed to the LIFT detector. This set-up ensured that both instruments observed leaves with the same field of view (FOV). Radiometric calibration of the QE Pro spectroradiometer was performed through the optical path of the LIFT instrument at the Commonwealth Scientific Industry Research Organisation's High Resolution Plant Phenomics Centre [24].

The LIFT instrument was operated with a non-invasive flash cycle (termed Q_A flash) [22] with an SQ_A phase consisting of 300 flashlets separated by a 1.6 µs delay (~3 ms) and an RQ_A phase consisting of 90 flashlets with an exponential increase in the 1.6 µs delay described by an exponential term of 0.5 (~300 ms). To obtain dark adapted reference Fm values, for the calculation of YNPQ and YNO, a modified flash cycle (termed PQ flash) with an SQ_A phase consisting of 6000 flashlets with a 20 µs delay and an RQ_A phase identical to the Q_A flash (~700 ms) was used [22]; see supplementary material, Figure S1 for comparison of the Q_A and PQ flash to PAM. To facilitate automatic targeting and monitoring of measured leaves, the LIFT and QE Pro were mounted on a computer controlled motorized tripod (Celestron advanced VX; Celestron, Rouse Hill, NSW, Australia) and operated through custom designed software.

2.3. Leaf Measurements

Measurements were performed on attached leaves fixed in a vertical position by taping the leaf tip to a wooden stake (avocado), or by fixing multiple leaves onto a black foam board target to produce a flat surface (orange jasmine). Leaf targets faced east at a distance of one meter from the LIFT fore optic. Measurements of active fluorescence and reflected solar radiance were performed in a semi-continuous fashion. Each cycle began with a white reference measurement (Spectralon,

Labsphere Inc., North Sutton, NH, USA), followed by a leaf measurement before returning to the white reference (Figure 1; see supplementary material; Video S1).

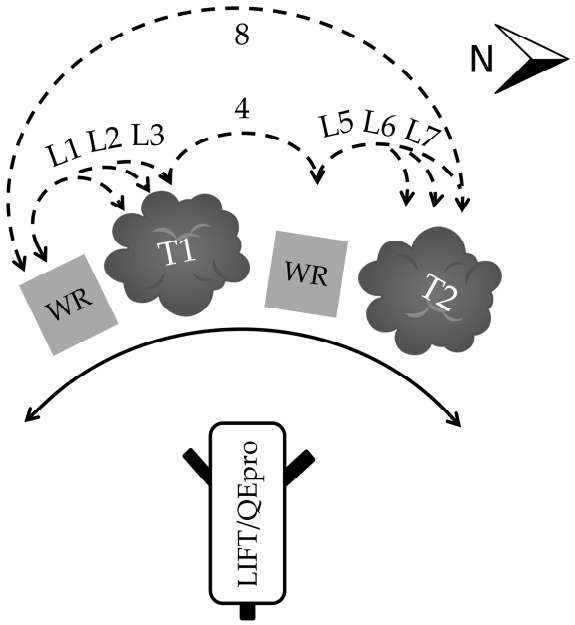

Figure 1. Nadir perspective of the diurnal measurement set-up with the Light Induced Fluorescence Transient instrument (LIFT) and QE Pro mounted on a motorized tripod and successively panned between two white reference panels (WR) and six different leaves on two trees (T1 and T2). The solid arc indicates the movement range of the tripod mounted LIFT and QE Pro. Broken arcs indicate the movements for successive measurements, where each arc indicates a single panning movement from WR to leaf and back to WR. The number labels on the broken lines indicate the sequence of panning movements, with those proceeded with an "L" indicating panning motions where leaf measurements occurred.

Each measurement consisted of a QE Pro reflected radiance measurement consisting of six 160 ms scans (440–870 nm), followed by a LIFT non-invasive Q_A flash measurement (500 ms; time for Q_A flash and transient fitting). Sequential leaf and white reference measurements resulted in a measurement resolution of approximately 3 min per leaf. These semi-continuous and sequential leaf measurements were repeated from dawn to dusk on cloud free and full sun days, with the set of six leaves changed daily over a total of 18 days. Six leaf replicates were chosen due to geometrical constraints of the tripod panning movements and to maximise the measurement frequency for each leaf. At UOW the 5 d of avocado and 8 d of orange jasmine measurements started 1 h before sunrise and concluded 2 h after sunset. Due to field power limitations the 5 d of avocado measurements at SHF had to be halted 2 h before sunset. Following diurnal measurements, dark-adapted Fm reference values were collected 30 min post sunset using the PQ flash protocol.

Simultaneously with LIFT/QE Pro measurements, leaf-level PAR was recorded at the surface of each leaf every 5 s using six LS-C micro quantum light sensors (Walz, Effeltrich, Germany) connected to two custom built data loggers (TriplePAR, Gademann Instruments, Würzburg, Germany). In addition, global PAR was recorded every 10 s using a sky facing MQS-B mini quantum sensor (Walz, Effeltrich, Germany) connected to a Universal Light Meter (ULM-500, Walz, Effeltrich, Germany). Following diurnal measurements, leaf thickness and Chl content measurements were collected at three inter-vein locations per leaf using Vernier calliper and a Soil–Plant Analyses Development 502 chlorophyll meter (SPAD, Spectrum Technologies Inc, Aurora, IL, USA), respectively. Leaf discs (1.5 cm^2 in diameter) were collected from adjacent non-monitored areas of avocado leaves for laboratory leaf pigment determination. Leaf discs were collected from each leaf pre-dawn at UOW. At SHF they were sampled

four times during each measurement day: pre-dawn, 1 h and 2 h after direct sunlight exposure, and post-sunset (n = 36 different leaves). Leaf discs were immediately frozen in liquid N_2 and stored at −80 °C pending pigment analysis.

2.4. Chlorophyll, Xanthophyll and Carotenoid Quantification

Chl *a* and *b*, xanthophyll pigments (violaxanthin, antheraxanthin and zeaxanthin), lutein, lutein epoxide and α- and β-carotene (α- and β-car) leaf contents were quantified using high performance liquid chromatography (HPLC; Shimadzu LC-10AT VP, Sydney, Australia). Pigments were extracted as described in Förster et al. [25] and quantified as described in Pogson et al. [26]. All pigment concentrations were normalized based on leaf disc area in $\mu g \cdot cm^{-2}$. Violaxanthin de-epoxidation status (DEPS), reflecting the extent to which the photoprotective xanthophyll cycle carotenoids are engaged, was calculated according to Gilmore and Björkman 1994 [27]:

$$\text{DEPS} = \frac{\text{antheraxanthin} + \text{zeaxanthin}}{\text{antheraxanthin} + \text{zeaxanthin} + \text{violaxanthin}} \quad (1)$$

Xanthophyll and lutein pool sizes were taken as the sums of violaxanthin, antheraxanthin and zeaxanthin (∑VAZ) and lutein and lutein epoxide (∑LLx) concentrations, respectively. Significant difference between pigment samples at different collection times was tested using ANOVA and Turkey HSD tests in the R software package [28].

2.5. Calculation of Photosynthetic Parameters

All parameters and symbols in this study match the conventional PAM terminology, with the LIFT data being marked by a Q_A or PQ to denote the source of the fluorescence data from either the Q_A or PQ flashes described previously [22]. Maximum photochemical yield of photosystem II was calculated as:

$$\phi\text{PSII}Q_A = \frac{(\text{Fm}Q_\text{A} - \text{Fo}Q_\text{A})}{\text{Fm}Q_\text{A}} \quad (2)$$

for a leaf in the dark and

$$\text{YPSII} = \frac{(\text{F}'\text{m}Q_\text{A} - \text{F}'Q_\text{A})}{\text{F}'\text{m}Q_\text{A}} \quad (3)$$

for a leaf in the light.

Electron transport rate (ETR) was calculated using the formula of Genty et al. [29]:

$$\text{ETR} = \text{YPSII} \times \text{PAR} \times E \times \alpha \quad (4)$$

where PAR was taken as the incident light intensity at the leaf surface and the energy partitioning between PSI and PSII (E) taken as 0.5 [3]. The leaf absorbance (α) was determined for each leaf from regression of leaf SPAD measurements against the PAR absorbance (400 to 700 nm) of leaves measured in an integrating sphere (see supplementary material; Figure S2). Partitioning of the yields of non-photochemical quenching (YNPQ) and constitutive heat dissipation (YNO) [22] were calculated according to the formulas of Klughammer et al. [30]:

$$\text{YNPQ} = \frac{\text{F}'Q_\text{A}}{\text{F}'\text{m}Q_\text{A}} - \frac{\text{F}'Q_\text{A}}{\text{FmPQ}} \quad (5)$$

And

$$\text{YNO} = \left(\frac{\text{F}'Q_\text{A}}{\text{FmPQ}}\right) \quad (6)$$

Note that

$$\text{YPSII} + \text{YNPQ} + \text{YNO} = 1 \quad (7)$$

Light use efficiency (LUE) was calculated using the formula of Rascher and Pieruschka [31]:

$$\text{LUE} = \frac{\text{Daily ETR}}{\text{Daily PAR}} \quad (8)$$

where daily ETR and daily PAR are calculated as the integrated area under curve (AUC) of the ETR and PAR for each diurnal measurement from sunrise until two hours before sunset.

2.6. Retrieval of Reflectance Indices and Solar Induced Fluorescence

As leaf and white reference reflectance measurements were not collected simultaneously, changes in ambient light intensity (typically caused by patchy cloud cover) occasionally resulted in a mismatch between reflected radiance measurements. To overcome this, simultaneous global PAR measurements were used to identify and match each leaf spectrum with a white reference counterpart taken within ±15 min. This time period was chosen, because changes in solar altitude were found to have a negligible effect on radiance computation during this time frame. The matching was performed in the R programming language and resulted in a mean absolute time mismatch ± standard deviation (SD) of 4.22 ± 4.89 min and a PAR mismatch of 7.89 ± 17.93 µmol photons·m^{-2}·s^{-1}, respectively. Leaf target measurements, where the closest matching white reference measurement differed in PAR by >10 µmol photons·m^{-2}·s^{-1}, were discarded.

NDVI, PRI and SIF at 687 (red) and 760 nm (far-red; FR) were retrieved from screened radiance data. The NDVI and PRI were calculated according to Rouse Jr. [32] and Gamon [15] respectively, using a 5 nm wavelength averaging. Since changes in SIF_{red} and SIF_{FR} were found to influence NDVI values, with a high SIF corresponding to increases in NDVI, the red reference wavelength was shifted to 647 nm and the FR reference wavelength was taken at 868 nm to minimise this influence. Retrieval of SIF was performed using the Fraunhofer Line Discriminator (FLD) [33] and the 3FLD [34] methodologies within both the O_2-A and O_2-B absorption spectral regions. Under low levels of leaf irradiance (<150 µmol photons·m^{-2}·s^{-1}), the 3FLD SIF retrieval occasionally resulted in negative estimates of SIF. As such, all negative SIF retrievals were reclassified to 0 mW·m^{-1}·sr^{-1}·nm^{-1}. Solar induced fluorescence yields (YSIF) for both the red and FR retrievals were calculated as the SIF value normalized to the absorbed PAR:

$$\text{YSIF}_\lambda = \frac{\text{SIF}_\lambda}{\text{APAR}} \quad (9)$$

where the APAR was calculated as the incident light intensity at the leaf surface multiplied by the absorbance of the leaf (400 to 700 nm).

2.7. Data Analyses

Daily correlations between SIF and other measured parameters were examined using linear regression performed in R [28]. Multiple regressions were performed separately for both species, with SIF_{FR}, SIF_{red}, $YSIF_{FR}$, and $YSIF_{red}$ as response variables, and all other measured parameters as predictors.

For analysis of seasonal trends multidimensional scaling (MDS) was used. The advantage of MDS analysis is that it reduces standardised daily measurements of many calculated photosynthetic parameters to a reduced set of dimensions, usually two, that enable visualisation of trends while still capturing the majority of the variance. Leaves with higher overall similarity in photosynthetic response will be closer together, and vectors can be placed to indicate which leaves are highest in each parameter. Raw fluorescence measurements of Fm, F'm, Fo and F', which are sensitive to small changes in distance between LIFT and target and incomparable between different leaf types and species, were excluded from analyses. Temporal measurement series collected with LIFT and QE Pro were smoothed using a centred moving average of the two previous and following measurements. Daily measurements were integrated as the AUC of each measured parameter, per leaf, for the period from sunrise until 2 h pre sunset. For leaf pigments, daily measurements were taken as the mean pigment concentrations

in $\mu g \cdot cm^{-2}$ averaged for the four daily samples at SHF. Additionally, daily maximum and minimum air temperatures were collected from Bureau of Meteorology, Australia weather stations situated 7.0 km (station number: 68,228) and 9.9 km (station number: 58,214) from UOW and SHF respectively. Standardization of each daily parameter was performed using z scores.

MDS analyses were performed in the R programming environment [28] using the packages: vegan [35] for calculation of Euclidean distances and Modern Applied Statistics with S (MASS) [36] for MDS analyses. MDS analyses were performed with both two- and three-dimensions separately for each species and with a combined data set. In each case, MDS were run on the following spectral and photosynthetic parameters: YPSII, ETR, YNO, YNPQ, SIF_{red}, SIF_{FR}, $YSIF_{red}$, $YSIF_{FR}$ NDVI, PRI and LUE, with vectors calculated for the spectral and photosynthetic parameters listed above, the environmental variables: day length, global PAR, leaf PAR, daily min air temperature and daily max air temperature (avocado and orange jasmine), and the leaf physical properties: leaf thickness, total Chl content, Chl a/b ratio, $\sum$VAZ, $\sum$LLx and α/β car ratio (avocado only). Separate MDS analyses of both species data with both two- and three-dimensions produced similar results, with two-dimensional MDS plots for the combined dataset found to adequately explain $\geq$84% of the variability in the data. For this reason, only results from two-dimensional MDS are presented here; results of three-dimensional MDS analysis can be found in the supplementary material (Figure S3 and Table S1).

3. Results

3.1. Seasonal Drivers of Solar Induced Fluorescence

Two-dimensional MDS analysis of seasonal SIF drivers (plot stress = 0.16) showed a clustering of orange jasmine data points, with a low dispersion and a small location shift (opposite to the vectors for LUE, YPSII and PRI) relative to avocado data points (Figure 2). Avocado data points from each day showed clustering relative to each another, having a larger dispersal than orange jasmine data points. High significance was found for the vectors for all spectral and photosynthetic variables ($p \leq 0.001$), with the exception of $YSIF_{red}$ ($p = 0.256$). Vectors for the environmental variables and leaf physical properties, particularly leaf thickness ($p \leq 0.001$), day length ($p \leq 0.001$), daily min air temperature ($p = 0.005$) and leaf PAR ($p \leq 0.001$), were all found to be significant, whereas vectors for all pigments were statistically insignificant.

Regarding the spectral and photosynthetic vectors, $YSIF_{FR}$ and SIF_{FR} were found to be tightly associated in the same direction as ETR. This $YSIF_{FR}$, SIF_{FR} and ETR vector grouping was found to be opposite to the tight grouping of $YSIF_{red}$, YNO and NDVI vectors. Independent to the SIFs, ETR, YNO and NDVI vectors, were the vectors for photosynthetic light use efficiency (LUE and YPSII) and stress (PRI and YNPQ), which formed two separate groups in opposing directions. The vectors for LUE and YPSII were associated with increasing PRI values (decreasing stress) and were in the opposite direction to the vector for YNPQ.

Vectors for the environmental variables and leaf physical properties were found to radiate only toward negative values of the Y axis. Tight grouping was found for the pigment vectors (total Chl, Chl a/b and $\sum$VAZ) and daily maximum temperature. Vectors for both global and leaf PARs were found to be tightly grouped in the same direction as $\sum$LLx. Unrelated to the vectors for global PAR, leaf PAR and $\sum$LLx were the vectors for leaf thickness and α/β car ratio, which were in an opposite direction to the vector for day length. The vector for daily minimum temperature was found in-between the vectors for leaf thickness, α/β car ratio and other leaf pigment vectors.

Comparing the two MDS plots, the significant SIF vectors were found in the same direction as the vectors for leaf and global PARs, leaf pigments (total Chl, Chl a/b and $\sum$VAZ) and daily maximum temperature. Opposite these vectors were the vectors for NDVI, YNO and $YSIF_{red}$. The vectors for LUE, PRI and YPSII, were in the same direction as the vectors for leaf thickness, α/β car ratio and minimum daily temperature, which were opposite the vector for YNPQ.

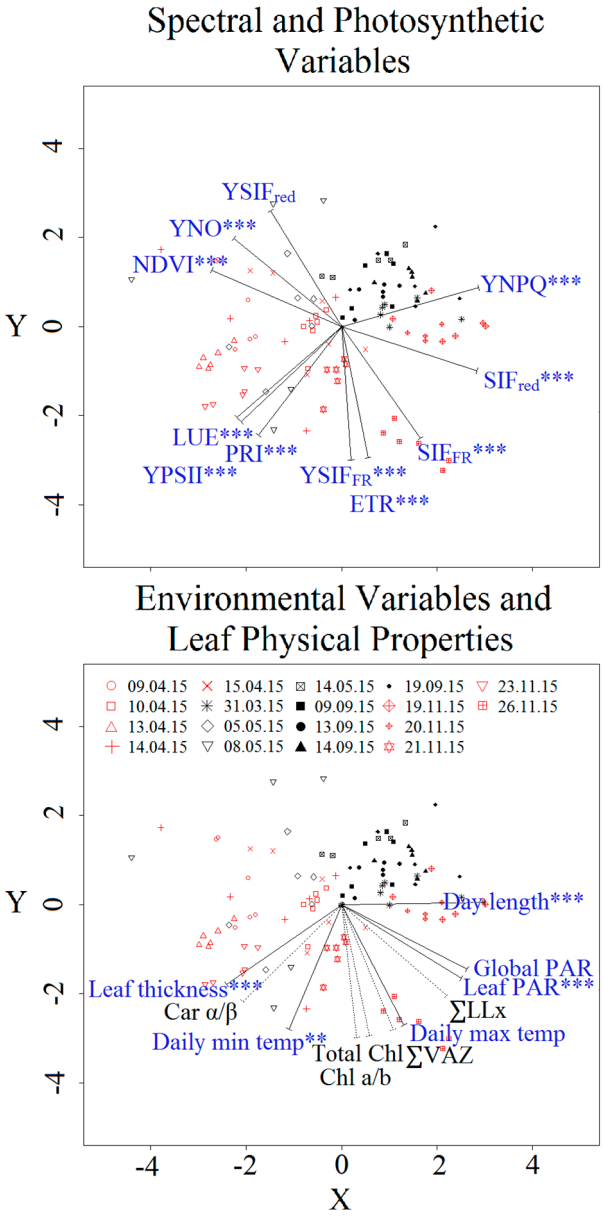

Figure 2. Two-dimensional multidimensional scaling (2D MDS) analysis of daily photosynthetic, physical, leaf pigment and remotely sensed measurements from leaves of avocado (red) and orange jasmine (black; stress = 0.16). Analyses were performed on the spectral and photosynthetic variables (electron transport rates (ETR), photosystem II yield (YPSII), non-photochemical quenching (YNPQ), constitutive heat dissipation (YNO), solar induced chlorophyll fluorescence (SIF); SIF_{red} and SIF_{FR}, $YSIF_{red}$ and $YSIF_{FR}$, light use efficiency (LUE), normalized difference vegetation index (NDVI) and photochemical reflectance index (PRI)), with vectors calculated for the spectral and photosynthetic variables, the environmental variables (day length, global photosynthetically active radiation (PAR), leaf PAR, daily min air temperature (daily min temp) and daily max air temperature (daily max temp)) and the leaf physical properties (leaf total chl, Chl a/b, ∑VAZ, ∑LLx, Car α/β, leaf thickness). Measurement dates are marked by symbol type, with dates given in day/month/year format in the legend. Data points between the 31.03.15 to 19.09.15 represent University of Wollongong, Ecology Research Centre (UOW) grown plants, whereas dates between 19.11.15 to 26.11.15 represent orchard grown plants from Summerland House Farm (SHF). Where data were available for both avocado and orange jasmine leaves, vectors are shown as solid lines and vector names are in blue. Where data was only available from avocado leaves (leaf pigments), vectors are shown as broken lines and vector names are in black. Significant vectors are marked by *, where *** $p < 0.001$ and ** $p \geq 0.001$ & $p < 0.01$. All vectors have been scaled by a factor of three to facilitate visualization.

3.2. Daily Drivers of Solar Induced Fluorescence

Correlations between daily measurements of SIF, photosynthesis and PAR were examined separately for avocado and orange jasmine using regressions of means for each time point (Table 1). Correlations with YSIF, where R^2 values were found to be very low ($R^2 < 0.01$) and figures for correlations where $R^2 < 0.1$ are not shown in text (see supplementary material; Table S2 and Figures S4–S6).

Table 1. Matrix table of p and R^2 values for correlations between SIF (red and far-red (FR)) and LIFT photosynthetic (ETR, YPSII, YNPQ, YNO), PAR (leaf and global) and spectral (PRI and NDVI) measurements, from two different species of plants (avocado (n = 1266) or orange jasmine (n = 986)), with measurements performed every 3 min and averaged for 6 leaves of each species. For each correlation the p value is given followed by the R^2 value in brackets; where insignificant, correlations are italicized. p values should be interpreted with caution due to pseudo-replication of measurements (3 min apart).

Measurement	Avocado p Values (R^2)		Orange Jasmine p Values (R^2)	
	SIF_{red}	SIF_{FR}	SIF_{red}	SIF_{FR}
Leaf PAR	<0.001 (0.52)	<0.001 (0.65)	<0.001 (0.14)	<0.001 (0.35)
Global PAR	<0.001 (0.05)	<0.001 (0.14)	<0.001 (0.03)	*0.315* (*<0.01*)
ETR	<0.001 (0.33)	<0.001 (0.28)	<0.001 (0.14)	<0.001 (0.18)
YPSII	<0.001 (0.39)	<0.001 (0.32)	<0.001 (0.18)	<0.001 (0.23)
YNPQ	<0.001 (0.10)	<0.001 (0.07)	<0.001 (0.14)	<0.001 (0.17)
YNO	<0.001 (0.48)	<0.001 (0.35)	<0.001 (0.27)	<0.001 (0.24)
PRI	0.003 (<0.01)	*0.914* (*<0.01*)	<0.001 (0.03)	<0.001 (0.05)
NDVI	<0.001 (0.03)	*0.202* (*<0.01*)	*0.610* (*0.01*)	0.001 (<0.01)

For raw SIF retrievals, significant correlations were found between SIF and all photosynthetic measurements (ETR, YPSII, YNPQ and YNO), both global and leaf PARs and PRI and NDVI, for both avocado and orange jasmine ($p < 0.005$); with the exception of NDVI ($p = 0.20$) and PRI for SIF_{FR} ($p = 0.91$) in avocado leaves and global PAR ($p = 0.32$) and NDVI ($p = 0.61$) for SIF_{FR} and SIF_{red} respectively in orange jasmine leaves (Figure 3). In avocado, positive correlations were found between both SIF_{FR} and SIF_{red} and leaf PAR, ETR and YNPQ, while strong negative correlations were identified between both SIF_{FR} and SIF_{red} and YPSII and YNO. The same correlations were identified for orange jasmine. However, in these cases the R^2 values were found to be lower (Figure 3), with the exception of the relationship between SIF_{red} and YNPQ.

Multiple regression models, run with SIF_{FR} as a response variable and all other parameters as predictors, consistently identified leaf PAR as the main significant predictor of SIF_{FR} ($p < 0.001$) for both species ($R^2 = 0.70$, avocado; and 0.45, orange jasmine). ETR ($p < 0.001$), NDVI ($p < 0.001$) and PRI ($p < 0.001$; avocado only) were also identified as significant predictors, but the contribution of other predictors to overall model improvement was negligible (improvement in $R^2 = 0.05$, avocado; and 0.09, orange jasmine). Leaf PAR was also identified as the main predictor of SIF_{red} for both species ($p < 0.001$; $R^2 = 0.64$, avocado and $p = 0.004$; $R^2 = 0.43$, orange jasmine). Additionally, YPSII ($p = 0.009$), global PAR ($p < 0.001$), ETR ($p < 0.001$), YNPQ ($p = 0.019$), YNO ($p = 0.009$) and NDVI ($p < 0.001$) were identified as significant SIF_{red} predictors for avocado, while NDVI ($p < 0.001$) was the only other significant SIF_{red} predictor for orange jasmine. However, unlike for SIF_{FR}, leaf PAR and NDVI as well as leaf PAR and global PAR were found to contribute substantially to avocado and orange jasmine SIF_{red} models respectively (improvement in $R^2 = 0.05$, avocado; and 0.09, orange jasmine). All other predictors contributed negligibly to model improvement. R^2 values were found to be low for all models run with SIF yields as response variables for both avocado ($R^2 = 0.11$, $YSIF_{FR}$; and 0.04, $YSIF_{red}$) and orange jasmine ($R^2 = 0.14$, $YSIF_{FR}$; and 0.04, $YSIF_{red}$).

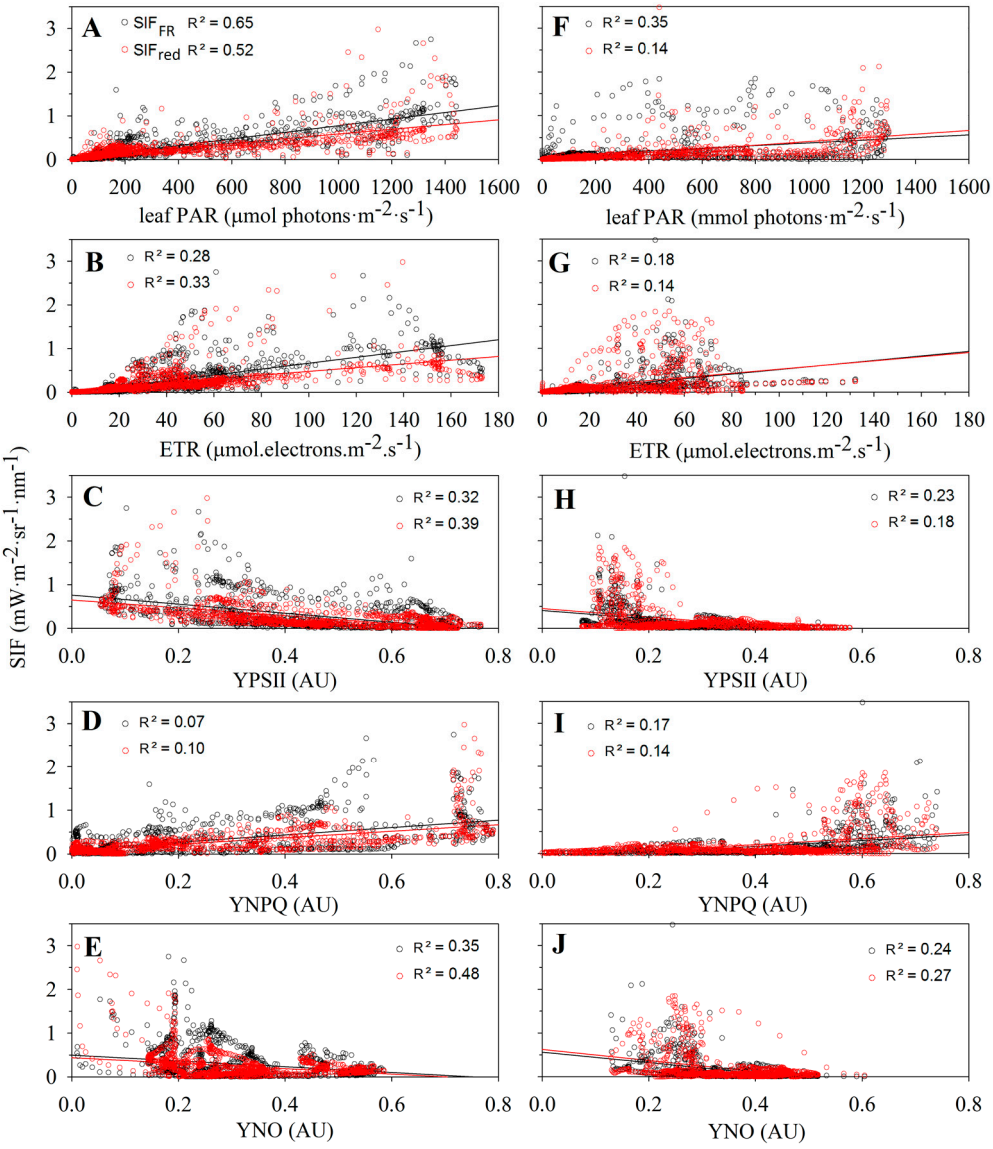

Figure 3. Scatterplots of leaf measurements of SIF_{red} (red) and SIF_{FR} (black) against LIFT measured photosynthetic parameters and leaf PAR from leaves of both avocado (**A**–**E**) and orange jasmine (**F**–**J**). LIFT and SIF measurements were collected simultaneously from sunrise to sunset with a three-minute time resolution. Plots show data from all time points and measurement days, where each point represents the mean of six leaf replicates collected at the same time on a single measurement day ±3 min. The black and red lines show the linear fit for SIF_{red} (red) and SIF_{FR} (black).

3.3. Diurnal Trends in Solar Induced Fluorescence

Values of SIF_{red} and SIF_{FR} for both avocado and orange jasmine leaves changed diurnally in response to increasing leaf PAR (Figure 4A,G). However, the relative rates of change in SIF and leaf PAR differed (Figure 4B,H). SIF was found to increase more rapidly than the increasing leaf PAR during first light exposure in the morning. A plateau or a decrease often followed this rapid SIF increase once maximum leaf PAR was reached. Both SIF_{red} and SIF_{FR} declined rapidly during the afternoon as leaf PAR decreased and thereafter remained low. Both species showed broadly similar diurnal SIF patterns. However, avocado leaves showed more consistent and less erratic diurnal changes in SIF and consistently higher values of both SIF_{red} and SIF_{FR}. Solar induced chlorophyll fluorescence yields changed little during slow diurnal changes in light intensity, with a tendency to be slightly higher in the morning and afternoon (Figure 4C,I). Fast changes in YSIF were commonly observed during

fluctuations in leaf PAR. Under these conditions SIF_{FR} decreases lagged behind leaf PAR decreases resulting in higher values of $YSIF_{FR}$. Conversely, for $YSIF_{red}$, changes were quite erratic and associated with large errors.

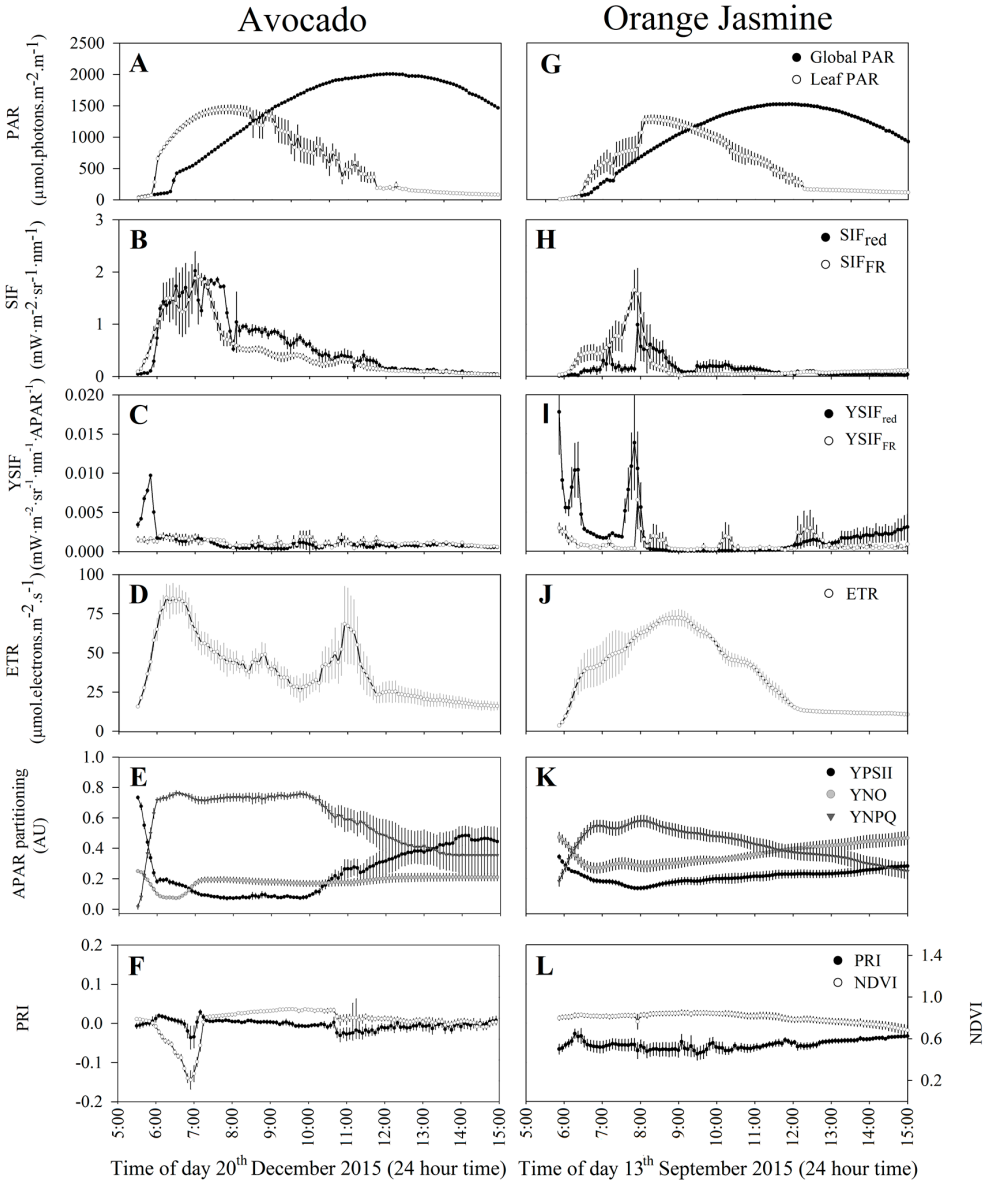

Figure 4. Diurnal changes in PAR, SIF, SIF yields, photosynthetic parameters and spectral indices measured using a LIFT instrument and QE Pro. The Y axis of each panel shows measured parameters as they change over a diurnal cycle. Each data point represents the mean ± SE (vertical bars) of six fully expanded avocado leaves from SHF (**A**–**F**) and orange jasmine leaves from UOW (**G**–**L**). All measurements were collected with a mean resolution of ~3 min ± 3 min per sample and have been smoothed using a centred moving average of the two following and previous measurements. Measurements from 20 December and 13 September 2015 have been selected as illustrative examples of commonly observed diurnal changes in measured parameters in the two examined plant species.

Changes in photosynthetic parameters were broadly consistent in behaviour across both plant species, with the exception of ETR. Electron transport rates for both leaves of avocado and orange jasmine were found to display similar maximum values (~50 µmol electons·m^{-2}·s^{-1}), but differ in behaviour (Figure 4D,J) during measurements at SHF. In avocado leaves, maximum ETR was achieved

during moderate light exposure in the morning and afternoon, with ETR decreasing or plateauing during the middle of the day (Figure 4D). Contrastingly, in orange jasmine, maximum ETR was consistently achieved during the middle of the day, with lower values of ETR during the morning and afternoon (Figure 4J). APAR partitioning in both species was strongly linked to leaf PAR (Figure 4E,K). However, the three yield components (YPSII, YNO and YNPQ) were observed to differ over the course of a day between avocado and orange jasmine leaves. In avocado, high morning leaf PAR resulted in a rapid increase in YNPQ to high levels (~0.8); this change coincided with a rapid decrease in YPSII to low levels (0.2 to 0.1) and a decrease in YNO from a steady value of ~0.2 to ~0.1 (Figure 4E). In orange jasmine, similar changes were observed during the morning increase in leaf PAR. However, changes in YNPQ, YPSII and YNO were not as pronounced, with YNPQ reaching maximum values of ~0.6, coinciding with a decrease in YPSII from 0.4 to 0.2 and a decrease in YNO from 0.5 to ~0.3 (Figure 4K). During high midday PAR, high levels of YNPQ and low levels of YPSII were maintained in leaves of both avocado and orange jasmine, with YNPQ subsequently decreasing and YPSII increasing with decreasing leaf PAR in the afternoon. Changes in YNO between the two species were found to differ in behaviour. In avocado leaves, the morning decrease in YNO was found to recover within ~1 h under high levels of leaf PAR (Figure 4E). However, in orange jasmine leaves YNO took much longer (~8 h) to recover, with recovery linked to decreases in leaf PAR in the afternoon and the recovery of YNPQ and YPSII (Figure 4K).

The reflectance indices showed relatively little change throughout the day (Figure 4F,L). However, changes in both PRI and NDVI were observed mainly in the morning, coinciding with rapid changes in intensities of solar illumination. Morning sudden decreases and increases in the reflectance indices were more apparent in avocado than in orange jasmine. Pigment analyses from avocado leaf discs sampled at different time points throughout the day (Table 2) show no significant changes in total Chl content or Chl a/b ratio throughout the day. Additionally, although significant changes in violaxanthin DEPS were observed ($p < 0.001$), no significant changes in PRI or NDVI were found.

Table 2. Leaf pigment composition and spectral indices measured from avocado leaf discs collected at one of four different time points: before sunrise (pre-dawn), 1 h (sunlight +1) and 2 h (sunlight +2) after direct sunlight exposure and after sunset. Leaf spectral indices (PRI and NDVI) were taken from diurnal measurement with a QE Pro spectroradiometer. Violaxanthin de-epoxidation status (DEPS), Chl a/b and total Chl were determined via HPLC, where total Chl is given in $\mu g \cdot cm^{-2}$. All data represents the mean ± SE (n = 30) of avocado leaf discs collected at SHF for each treatment. Significant differences between treatments are marked by ***. Treatments not connected by the same letter are significantly different.

Treatment	Pre-Dawn	Sunlight +1	Sunlight +2	After Sunset
Pigment/spectral Indices				
PRI	−0.0022 ± 0.0028	0.011 ± 0.0035	0.00038 ± 0.0062	0.0018 ± 0.0078
NDVI	0.73 ± 0.035	0.73 ± 0.034	0.73 ± 0.051	0.75 ± 0.035
DEPS ***	0.21 ± 0.021 ^{A}	0.49 ± 0.046 ^{B}	0.53 ± 0.048 ^{B}	0.27 ± 0.039 ^{A}
Total Chl	58.88 ± 3.95	69.86 ± 5.27	60.94 ± 4.45	64.34 ± 3.86
Chl a/b	2.41 ± 0.043	2.55 ± 0.057	2.56 ± 0.062	2.59 ± 0.056

4. Discussion

In recent years SIF has been proposed as a means to estimate terrestrial vegetation photosynthetic rates at multiple spatial scales, ranging from the leaf and canopy [5–8] to global scales [9–12]. However, changes in SIF fluctuate with the relative proportions of APAR used by plants for photochemistry or NPQ and as such, information about these parameters is needed to interpret SIF [14]. Although direct measurements of YPSII and YNPQ cannot be made over large spatial scales using passive remote sensing, they can be measured at leaf and small canopy levels with active fluorescence approaches and combined with passive observations. A few studies have investigated changes in SIF at small spatial scales in relation to active fluorescence measurements. However, they have either

involved broad-band SIF measurements, with a full width half maximum (FWHM) >1 nm, that are not comparable to the narrow-band SIF (FWHM < 1 nm) retrieved with spectral infilling approaches (i.e., FluorPen) [37], or have compared small canopy scale measurements with PAM measurements on single leaves [8,21]. Our approach goes in the same direction as these experiments; however, we focus exclusively on the leaf-level in order to avoid spatial mismatches between SIF and active fluorescence measurements. Using this approach, our data shows differences in the relationships between SIF and LIFT photosynthetic measurements in seasonal as well as daily regimes, which may be of importance for the interpretation of large spatial and temporal scale SIF measurements.

4.1. Seasonal Drivers of Solar Induced Fluorescence

Seasonal relationships between SIF and other measured parameters were relatively consistent between raw and yield values of SIF. Previous studies suggested that SIF_{FR} correlates with Chl content [38], NDVI [39], crop developmental stage [8], canopy and air temperatures [21], PAR [38] and F′ [7] over seasonal time scales. We found significant associations between changes in SIF_{FR}, SIF_{red} and $YSIF_{FR}$ with changes in leaf PAR, ETR and YNO. The relationship between SIF and ETR has been reported at global scales [17], but has not previously been reported at the leaf-level. Additionally, to the authors' knowledge, no study has indicated the relationship between SIF and YNO. YNO is thought to represent energy losses due to both fluorescence and constitutive heat dissipation [20]. However, we identified decreases in SIF with increases in YNO. This suggests that the dominant driver of YNO change was increases in constitutive heat loss, which may lead to reductions of SIF at seasonal time scales.

Our results also indicate potential relationships between increases in the SIF_{FR}, $YSIF_{FR}$ and SIF_{red} and increase in leaf pigment parameters, i.e., total Chl, Chl a/b, $\sum$VAZ and $\sum$LLx. Although the vector changes for leaf pigments were statistically insignificant ($p > 0.16$), with a larger pigment sample set it is likely that vectors for total Chl content and Chl a/b ratio may become significant. Unlike other pigment vectors the vector for car α/β ratio appeared to be associated with changes in leaf thickness and measurements of leaf stress and photosynthetic efficiency (LUE, YPSII and PRI). The further association of the stress and photosynthetic efficiency vectors with day length suggests that the relationship may be linked to seasonal changes in leaf longevity. During longer days (spring and summer) avocado plants produce new young leaves, which typically have a lower leaf thickness and a lower car α/β ratio, but greater capacity for photo-protection (YNPQ) [40].

Additionally, we also found a significant association between increases in SIF_{FR}, $YSIF_{FR}$ and SIF_{red} and decreases in NDVI. Interestingly, the direction of the vector for NDVI is opposing the vector direction for leaf total Chl content and it is unrelated to changes in leaf thickness, both of which are known causes of leaf NDVI changes [16]. This may suggest that the variability in NDVI values caused by seasonal changes in diffuse vs. specular irradiance, and/or other confounding factors, may be greater than the measured NDVI changes due to phenological fluctuations in Chl and leaf thickness. Contrastingly, seasonal association of low PRI values with high LUE and PSII yields is congruent with previously published findings [18,41,42]. Moreover, the vectors for LUE, PRI and YPSII also showed the expected relationship with YNPQ, where high values of NPQ correspond with lower LUE, YPSII and increasing (positive) PRI values (lower DEPS) [18].

4.2. Daily Correlations between Solar Induced Fluorescence

In this study we identified strong linear relationships between time resolved measurements of leaf PAR, SIF and photosynthesis in both plant species. Similar measurements performed by Pinto et al. [8] identified correlations between SIF_{FR} and PAR and ϕPSII, but found no unique relationship between the PAM measurements and PAR. We suggest that this may result from using reflectance and global PAR measurements, which were not able to accurately approximate the leaf-level PAR. We identified significant correlations between SIF and global PAR for avocado and orange jasmine leaves. Nonetheless, this relationship was of poor quality ($R^2 < 0.15$; Table 1), which suggests that

global PAR may be a poor proxy of true leaf PAR, at least in our situation, where leaves were oriented vertically in an east facing direction. Additionally, multiple regression consistently identified leaf PAR as a main predictor of SIF for both plant species, suggesting that collinearity between leaf PAR, photosynthesis and SIF is the main driver of correlations between SIF and photosynthesis within daily measurements.

To the best of our knowledge, no study has examined the relationship between APAR partitioning parameters (YPSII, YNO and YNPQ) and SIF and YSIF. We identified statistically significant correlations between SIF and YSIF with measurements of YPSII, YNPQ and YNO, and also global and leaf PARs (see supplementary material; Table S5). Correlations between SIF and YSIF with PAM measured F′ and ϕPSII or YPSII have been reported in both herbaceous plants and conifers [7,21,43]. However, the poor quality of relationships identified between YSIF and APAR partitioning parameters in this study suggests that further investigation may be required. Between the two species examined, correlations were of a lower significance for orange jasmine leaves. A strong waxy layer on the top adaxial side of orange jasmine leaves likely contributed to this by causing specular reflections and reducing the amount of absorbed excitation energy from LIFT flashes thereby increasing measurement errors. The direction of correlations between SIF and photosynthetic measurements were consistent with published correlations between SIF and ϕPSII and F′ (e.g., [7,8]) and were congruent with expected changes in YPSII, YNPQ, YNO and ETR under increasing leaf PAR.

4.3. Daily Trends in Solar Induced Fluorescence

The diurnal trends of both avocado and orange jasmine leaves showed the expected changes in photosynthetic parameters associated with changes in PAR. However, the two species differed in the magnitude of these changes. To our knowledge, there is no literature on active fluorescence measurement of orange jasmine available. As such, it is difficult to gauge if the lower YPSII and YNPQ of orange jasmine leaves in comparison to avocado leaves are triggered by physiological differences between the species. Moreover, differences in YPSII and YNPQ between the two species may be influenced by the mounting of orange jasmine leaves to a foam board target, which may have interfered with air flow and leaf temperature. For avocado, a few studies focusing on light adaptation and lutein cycle dynamics in avocado have reported PAM [25,44] and LIFT [31] estimates of YPSII and ETR similar to those reported under the comparable light conditions in this study.

Diurnal SIF changes of both plant species were found to occur in three discrete stages, as previously reported in canopy measurements of maize by Pinto et al. [8]. Morning SIF increases were often followed by a decrease, which was particularly evident in measurements of avocado leaves. No coincident changes in photosynthetic parameters were present during the SIF decrease. However, coincident changes in both NDVI and PRI, which were more pronounced in avocado leaves, were present. Since no changes in photosynthetic measurements or light conditions coincide with these decreases, we hypothesise that they correspond to solar geometries, where direct specular leaf reflections that are not present in measurements of the Lambertian white reference result in distortion of the optical indices and depth of O_2-A and O_2-B absorption features. It should, however, be noted that the behaviour of SIF_{red} was found to be less reliable, because of bigger associated errors and occasionally erratic behaviour that can be attributed to the shallower depth of the O_2-B absorption feature [6,45].

The photosynthetic parameters (ETR, YNO, YNPQ and YPSII) behaved as would be expected, with changes in avocado measurements similar to measurements of YPSII, ETR and NPQ reported by Rascher and Pieruschka [31]. Maximum light utilization (as measured by ETR) in avocado leaves occurred under moderate light in the morning and afternoon. The high light periods were dominated by low YPSII, high YNPQ and lower ETR. In contrast, peak light utilization in leaves of orange jasmine occurred during the middle of the day under high light. The decrease in ETR observed under the high light in some avocado measurements is indicative of reversible acute water stress and increased photorespiration that can occur during stomatal closure [46]. This is also evident in maximum rates

of YNPQ identified in avocado, which responded faster and reached higher levels than in orange jasmine, indicating better low light utilization and an occurrence of light stress under high levels of illumination. Additionally, differences in constitutive heat dissipation (YNO) were recorded between the two examined species. In situations when YNPQ and YPSII can regulate disposal of excess APAR, YNO may remain constant [20]. In leaves of avocado YNO remained constant throughout the day, with the exception of the rapid onset of direct irradiance in the morning, which caused a transient decrease in YNO. This decrease in YNO is indicative of a light induction, where the fast increase in light exceeds the slower increasing quenching capacity of YNPQ up-regulation. In contrast, YNO in orange jasmine leaves dropped during morning increases in light and slowly recovered with decreasing light in the afternoon. These fluctuations in YNO may suggest that under high irradiances APAR exceeds the quenching capacity of YPSII and YNPQ with the excess energy regulated through YNO. The observed differences in maximum light utilization between avocado and orange jasmine illustrate the physiological adaptations in photosynthetic regulation between the small and highly waxy orange jasmine foliage and large chlorophyll rich avocado leaves.

4.4. Correlations between NDVI, PRI and Leaf Pigments

Diurnal trends of NDVI and PRI showed no significant changes, with the exception of the aforementioned decreases during the morning. As expected, pigment sampling of avocado leaves at SHF showed no significant diurnal changes, with the exception of the photoprotective xanthophyll pigments (i.e., increase in zeaxanthin and decrease in violaxanthin). Significant increases in the DEPS at each sampling time point confirmed the engagement of slowly reversible photoprotective mechanisms one and two hours after direct illumination and recovery to lower levels by sunset. These changes in xanthophyll pigments are expressed in the PRI index [15]. Published leaf-level experiments have presented correlations between PRI, DEPS and NPQ [47]. PRI has also been shown to track changes in DEPS under stable chlorophyll and carotenoid concentration [21,38,48]. The morning decrease in PRI observed here corresponded with a significant DEPS increase in avocado leaf samples sampled one hour after light exposure. However, the high DEPS was found to be maintained in avocado leaf samples collected two hours following light exposure, whereas during this period PRI had returned to the pre-exposure level. This suggests that observed morning changes in PRI were not representing changes in xanthophyll composition. We hypothesise that it may be related to the physical and optical properties of avocado leaves, which require more detailed examination based on dedicated experiments. Unchanged daily leaf chlorophyll content indicates that the photosynthetic pigments could not be responsible for the significant morning decrease in NDVI observed for avocado leaves. Therefore, the morning drop, seen in both NDVI and PRI, does not result from plant physiological processes, but a temporal measurement error. We deduced that it is most likely caused by the LIFT instrument casting a light shadow on sampling spots during the early morning hours. The intensity differences between white reference and sample reflectance measurements subsequently triggered the variability in optical indices.

5. Conclusions

Our results show strong correlations between both SIF_{FR} and SIF_{red} and PAR ($p < 0.001$) and photosynthetic measurements (YPSII, YNPQ, YNO and ETR; $p < 0.001$) performed with the LIFT instrument over a diurnal cycle. When analysing measurements at seasonal scales, our results suggest that SIF indicates changes in ETR, YNO and leaf PAR, with all other changes being potentially explained by fluctuations in leaf pigments and maximum daily air temperature. Statistical analyses also suggest that short-term correlations between photosynthesis and SIF changes may be principally driven by collinearity between SIF and photosynthesis changes triggered by leaf PAR fluctuations.

This study demonstrates one of the first operational simultaneous SIF and active chlorophyll fluorescence proximal remote sensing, thus allowing statistically significant linkage of SIF with ETR and YNO. Overall, our results indicate that leaf level correlations observed over diurnal time scales

may not be present in seasonal trends, where longer term changes in plant pigments, temperature and irradiance become influential. However, the extent to which the observed leaf level correlations can be scaled to the top of canopy (TOC) using, for instance, a combination of an airborne variant of LIFT [49,50] and canopy radiative transfer modelling [51,52], requires further investigation. At TOC we would expect lower SIF_{red} due to reabsorption by canopy elements containing PAR absorbing pigments [53]. As such, leaf level SIF_{red} correlations may be weakened or not present at larger spatial scales. Additionally, SIF is commonly thought to be isotropically emitted from the leaf, making SIF retrieved at the leaf level minimally influenced be changes in solar irradiance and sensor viewing angularity [54]. At the canopy level SIF observations are strongly influenced by the angles between sun, foliage and measuring instruments [8,54]. This means that leaf level diurnal SIF changes will be very likely different at TOC. Nevertheless, TOC relationships between ϕPSII, ETR and SIF published recently [7,17,43] suggest that novel leaf level correlations between YNO and SIF_{FR}, identified in this study, may possibly hold at larger spatial scales, warranting future dedicated scaling experiments to test this hypothesis.

Supplementary Materials: Supplementary material may be found online at www.mdpi.com/2072-4292/9/6/604/s1, Figure S1: Relationship between PAM and LIFT measured YPSII calculated from Q_A and PQ flashes, Figure S2: Relationship between leaf absorbance (400 to 700 nm) and leaf SPAD optical density measurements for avocado and orange jasmine leaves, Figure S3: 3D MDS analysis of seasonal changes in LIFT and QE Pro measurements, Figure S4: Scatterplots of daily measurements of SIF_{red} and SIF_{FR} against global PAR, NDVI and PRI from leaves of avocado and orange jasmine, Figure S5: Scatterplots of daily measurements of YSIFred and YSIFFR against LIFT measured photosynthetic parameters and leaf PAR from leaves of both avocado and orange jasmine, Figure S6: Scatterplots of daily measurements of $YSIF_{red}$ and $YSIF_{FR}$ against global PAR, NDVI and PRI from leaves of avocado and orange jasmine, Table S1: Matrix table of the smallest absolute angles between vectors from 3D MDS analysis, Table S2: Matrix table of p values and R2 values for correlations between YSIF (red and FR) and LIFT and QE Pro measurements, Video S1: Time-lapse of LIFT and QE Pro diurnal measurements.

Acknowledgments: This project was supported by an Australian Research Council Discovery grant "AirLIFT" (DP140101488) and conducted in research facilities and with scientific equipment from the UOW and the Australian National University, with technical support for the LIFT instrument kindly provided by Zbigniew Kolber. We thank Chris Smith and the staff of SHF for allowing access to the orchard avocado trees and providing support for field measurements. We also thank Johanna Turnbull for her assistance in measurements at UOW and Melinda Waterman (M.W.) for assistance operating the HPLC and running pigment extracts. Lastly we are grateful to all the colleagues and collaborators who provided feedback on results and the manuscript. This research was completed as part of RWs PhD and partially funded through an Australian Government Research Training Program Scholarship and funding received by BO from the UOW.

Author Contributions: Z.M. and R.W. conceived the study, performed measurements at the UOW, collected leaf optical properties and performed the calibration and set-up of LIFT/QE Pro instrument. R.W. and B.O. collected measurements at SHF. Z.M. and R.W. developed a processing pipeline for analysis of LIFT and QE Pro measurement, with Z.M. providing retrievals of SIF and spectral indices and R.W. providing retrieval and normalization of LIFT/PAR data. Leaf pigments were analyzed by R.W. Analysis of completed datasets was performed by R.W. and M.A. R.W. wrote the manuscript and all authors (R.W., Z.M., M.A., B.O. and S.A.R.) contributed to interpretation of results and production of the manuscript.

Conflicts of Interest: The authors declare no conflict of interest.

References

1. Field, C.B.; Barros, V.R.; Dokken, D.J.; Mach, K.J.; Mastrandrea, M.D.; Bilir, T.E.; Chatterjee, M.; Ebi, K.L.; Estrada, Y.O.; Genova, R.C.; et al. Climate Change 2014: Impacts, Adaptation, and Vulnerability. Part A: Global and Sectoral Aspects. In *Contribution of Working Group II to the Fifth Assessment Report of the Intergovernmental Panel on Climate Change*; Cambridge University Press: Cambridge, UK, 2014.
2. Rascher, U.; Blossfeld, S.; Fiorani, F.; Jahnke, S.; Jansen, M.; Kuhn, A.J.; Matsubara, S.; Märtin, L.L.; Merchant, A.; Metzner, R. Non-invasive approaches for phenotyping of enhanced performance traits in bean. *Funct. Plant Biol.* **2011**, *38*, 968–983. [CrossRef]
3. Maxwell, K.; Johnson, G.N. Chlorophyll fluorescence—A practical guide. *J. Exp. Bot.* **2000**, *51*, 659–668. [CrossRef] [PubMed]

4. Nichol, C.J.; Pieruschka, R.; Takayama, K.; Förster, B.; Kolber, Z.; Rascher, U.; Grace, J.; Robinson, S.A.; Pogson, B.; Osmond, B. Canopy conundrums: Building on the Biosphere 2 experience to scale measurements of inner and outer canopy photoprotection from the leaf to the landscape. *Funct. Plant Biol.* **2012**, *39*, 1–24. [CrossRef]
5. Damm, A.; Elbers, J.; Erler, A.; Gioli, B.; Hamdi, K.; Hutjes, R.; Kosvancova, M.; Meroni, M.; Miglietta, F.; Moersch, A. Remote sensing of sun-induced fluorescence to improve modeling of diurnal courses of gross primary production (GPP). *Glob. Chang. Biol.* **2010**, *16*, 171–186. [CrossRef]
6. Rossini, M.; Meroni, M.; Celesti, M.; Cogliati, S.; Julitta, T.; Panigada, C.; Rascher, U.; van der Tol, C.; Colombo, R. Analysis of Red and Far-Red Sun-Induced Chlorophyll Fluorescence and Their Ratio in Different Canopies Based on Observed and Modeled Data. *Remote Sens.* **2016**, *8*, 412. [CrossRef]
7. Cendrero-Mateo, M.P.; Moran, M.S.; Papuga, S.A.; Thorp, K.; Alonso, L.; Moreno, J.; Ponce-Campos, G.; Rascher, U.; Wang, G. Plant chlorophyll fluorescence: Active and passive measurements at canopy and leaf scales with different nitrogen treatments. *J. Exp. Bot.* **2016**, *67*, 275–286. [CrossRef] [PubMed]
8. Pinto, F.; Damm, A.; Schickling, A.; Panigada, C.; Cogliati, S.; Müller-Linow, M.; Balvora, A.; Rascher, U. Sun-induced chlorophyll fluorescence from high-resolution imaging spectroscopy data to quantify spatio-temporal patterns of photosynthetic function in crop canopies. *Plant Cell Environ.* **2016**. [CrossRef] [PubMed]
9. Guan, K.; Berry, J.A.; Zhang, Y.; Joiner, J.; Guanter, L.; Badgley, G.; Lobell, D.B. Improving the monitoring of crop productivity using spaceborne solar-induced fluorescence. *Glob. Chang. Biol.* **2016**, *22*, 716–726. [CrossRef] [PubMed]
10. Zhang, Y.; Guanter, L.; Berry, J.A.; Joiner, J.; van der Tol, C.; Huete, A.; Gitelson, A.; Voigt, M.; Köhler, P. Estimation of vegetation photosynthetic capacity from space-based measurements of chlorophyll fluorescence for terrestrial biosphere models. *Glob. Chang. Biol.* **2014**, *20*, 3727–3742. [CrossRef] [PubMed]
11. Guanter, L.; Zhang, Y.; Jung, M.; Joiner, J.; Voigt, M.; Berry, J.A.; Frankenberg, C.; Huete, A.R.; Zarco-Tejada, P.; Lee, J.-E. Global and time-resolved monitoring of crop photosynthesis with chlorophyll fluorescence. *Proc. Natl. Acad. Sci. USA* **2014**, *111*, 1327–1333. [CrossRef] [PubMed]
12. Joiner, J.; Yoshida, Y.; Vasilkov, A.; Middleton, E. First observations of global and seasonal terrestrial chlorophyll fluorescence from space. *Biogeosciences* **2011**, *8*, 637–651. [CrossRef]
13. Porcar-Castell, A.; Tyystjärvi, E.; Atherton, J.; van der Tol, C.; Flexas, J.; Pfündel, E.E.; Moreno, J.; Frankenberg, C.; Berry, J.A. Linking chlorophyll a fluorescence to photosynthesis for remote sensing applications: Mechanisms and challenges. *J. Exp. Bot.* **2014**, *65*, 4065–4095. [CrossRef] [PubMed]
14. Schlau-Cohe, G.S.; Berry, J. Photosynthetic fluorescence, from molecule to planet. *Phys. Today* **2015**, *68*, 66. [CrossRef]
15. Gamon, J.A.; Serrano, L.; Surfus, J.S. The photochemical reflectance index: An optical indicator of photosynthetic radiation use efficiency across species, functional types, and nutrient levels. *Oecologia* **1997**, *112*, 492–501. [CrossRef] [PubMed]
16. Sims, D.A.; Gamon, J.A. Relationships between leaf pigment content and spectral reflectance across a wide range of species, leaf structures and developmental stages. *Remote Sens. Environ.* **2002**, *81*, 337–354. [CrossRef]
17. Zhang, Y.; Xiao, X.; Jin, C.; Dong, J.; Zhou, S.; Wagle, P.; Joiner, J.; Guanter, L.; Zhang, Y.; Zhang, G.; et al. Consistency between sun-induced chlorophyll fluorescence and gross primary production of vegetation in North America. *Remote Sens. Environ.* **2016**, *183*, 154–169. [CrossRef]
18. Rahimzadeh-Bajgiran, P.; Munehiro, M.; Omasa, K. Relationships between the photochemical reflectance index (PRI) and chlorophyll fluorescence parameters and plant pigment indices at different leaf growth stages. *Photosynth. Res.* **2012**, *113*, 261–271. [CrossRef] [PubMed]
19. Schickling, A.; Matveeva, M.; Damm, A.; Schween, J.H.; Wahner, A.; Graf, A.; Crewell, S.; Rascher, U. Combining Sun-Induced Chlorophyll Fluorescence and Photochemical Reflectance Index Improves Diurnal Modeling of Gross Primary Productivity. *Remote Sens.* **2016**, *8*, 574. [CrossRef]
20. Kramer, D.M.; Johnson, G.; Kiirats, O.; Edwards, G.E. New fluorescence parameters for the determination of Q_A redox state and excitation energy fluxes. *Photosynth. Res.* **2004**, *79*, 209–218. [CrossRef] [PubMed]
21. Ni, Z.; Liu, Z.; Huo, H.; Li, Z.-L.; Nerry, F.; Wang, Q.; Li, X. Early water stress detection using leaf-level measurements of chlorophyll fluorescence and temperature data. *Remote Sens.* **2015**, *7*, 3232–3249. [CrossRef]

22. Osmond, B.; Chow, W.S.; Wyber, R.; Zavaleta, A.; Keller, B.; Pogson, B.; Robinson, A.S. Relative functional and optical absorption cross sections of PSII and other photosynthetic parameters monitored in situ, at a distance with a time resolution of a few seconds, using a prototype Light Induced Fluorescence Transient (LIFT) device. *Funct. Plant Biol.* **2017**, in press.
23. Kolber, Z. *Light Induced Fluorescence Transient–Fast Repetition Rate (LIFT-FRR) Fluorometer Operating Manual*; Soliense Inc.: Santa Cruz, CA, USA, 2014.
24. Lucieer, A.; Malenovský, Z.; Veness, T.; Wallace, L. HyperUAS—Imaging spectroscopy from a multirotor unmanned aircraft system. *J. Field Robot.* **2014**, *31*, 571–590. [CrossRef]
25. Förster, B.; Osmond, C.B.; Pogson, B.J. De Novo Synthesis and Degradation of Lx and V Cycle Pigments during Shade and Sun Acclimation in Avocado Leaves. *Plant Physiol.* **2009**, *149*, 1179–1195. [CrossRef] [PubMed]
26. Pogson, B.; McDonald, K.A.; Truong, M.; Britton, G.; DellaPenna, D. Arabidopsis carotenoid mutants demonstrate that lutein is not essential for photosynthesis in higher plants. *Plant Cell.* **1996**, *8*, 1627–1639. [CrossRef] [PubMed]
27. Gilmore, A.M.; Björkman, O. Adenine nucleotides and the xanthophyll cycle in leaves. *Planta* **1994**, *192*, 526–536. [CrossRef]
28. R Core Team. *R: A Language and Environment for Statistical Computing*; R Foundation for Statistical Computing: Vienna, Austria, 2013.
29. Genty, B.; Briantais, J.-M.; Baker, N.R. The relationship between the quantum yield of photosynthetic electron transport and quenching of chlorophyll fluorescence. *(BBA) Gen. Subj.* **1989**, *990*, 87–92. [CrossRef]
30. Klughammer, C.; Schreiber, U. Complementary PS II quantum yields calculated from simple fluorescence parameters measured by PAM fluorometry and the Saturation Pulse method. *PAM Appl. Notes* **2008**, *1*, 27–35.
31. Rascher, U.; Pieruschka, R. Spatio-temporal variations of photosynthesis: The potential of optical remote sensing to better understand and scale light use efficiency and stresses of plant ecosystems. *Precis. Agric.* **2008**, *9*, 355–366. [CrossRef]
32. Rouse, J., Jr. *Monitoring the Vernal Advancement and Retrogradation (Green Wave Effect) of Natural Vegetation*; Texas A & M University, Remote Sensing Centre: Houston, TX, USA, 1974; pp. 1–10.
33. Carter, G.; Theisen, A.; Mitchell, R. Chlorophyll fluorescence measured using the Fraunhofer line-depth principle and relationship to photosynthetic rate in the field. *Plant Cell Environ.* **1990**, *13*, 79–83. [CrossRef]
34. Maier, S.W.; Günther, K.P.; Stellmes, M. Sun-induced fluorescence: A new tool for precision farming. In *Digital Imaging and Spectral Techniques: Applications to Precision Agriculture and Crop Physiology*; McDonald, M., Schepers, J., Tartly, L., Toai, T.V., Major, D., Eds.; American Society of Agronomy Special Publication: Madison, WI, USA, 2003; pp. 209–222.
35. Oksanen, J.; Blanchet, F.; Kindt, R.; Legendre, P.; Minchin, P.; O'Hara, R.; Simpson, G.; Solymos, P.; Stevens, M.; Wagner, H. Vegan: Community Ecology Package. R Package Vegan, Vers. 2.2-1; 2015. Available online: https://cran.r-project.org/web/packages/vegan/index.html (accessed on 3 July 2016).
36. Venables, W.N.; Ripley, B.D. *Modern Applied Statistics with S*, 4th ed.; Springer: New York, NY, USA, 2002.
37. Zarco-Tejada, P.; González-Dugo, M.; Fereres, E. Seasonal stability of chlorophyll fluorescence quantified from airborne hyperspectral imagery as an indicator of net photosynthesis in the context of precision agriculture. *Remote Sens. Environ.* **2016**, *179*, 89–103. [CrossRef]
38. Louis, J.; Ounis, A.; Ducruet, J.-M.; Evain, S.; Laurila, T.; Thum, T.; Aurela, M.; Wingsle, G.; Alonso, L.; Pedros, R. Remote sensing of sunlight-induced chlorophyll fluorescence and reflectance of Scots pine in the boreal forest during spring recovery. *Remote Sens. Environ.* **2005**, *96*, 37–48. [CrossRef]
39. Cogliati, S.; Rossini, M.; Julitta, T.; Meroni, M.; Schickling, A.; Burkart, A.; Pinto, F.; Rascher, U.; Colombo, R. Continuous and long-term measurements of reflectance and sun-induced chlorophyll fluorescence by using novel automated field spectroscopy systems. *Remote Sens. Environ.* **2015**, *164*, 270–281. [CrossRef]
40. Matsubara, S.; Naumann, M.; Martin, R.; Nichol, C.; Rascher, U.; Morosinotto, T.; Bassi, R.; Osmond, B. Slowly reversible de-epoxidation of lutein-epoxide in deep shade leaves of a tropical tree legume may 'lock-in' lutein-based photoprotection during acclimation to strong light. *J. Exp. Bot.* **2005**, *56*, 461–468. [CrossRef] [PubMed]
41. Wu, C.; Liu, Z.; Xu, S. Remote sensing of crop light use efficiency using photochemical reflectance index. *IEEE Trans. Geosci. Remote Sens.* **2016**, 1719–1722. [CrossRef]

42. Trotter, G.; Whitehead, D.; Pinkney, E. The photochemical reflectance index as a measure of photosynthetic light use efficiency for plants with varying foliar nitrogen contents. *Int. J. Remote Sens.* **2002**, *23*, 1207–1212. [CrossRef]
43. Meroni, M.; Rossini, M.; Picchi, V.; Panigada, C.; Cogliati, S.; Nali, C.; Colombo, R. Assessing steady-state fluorescence and PRI from hyperspectral proximal sensing as early indicators of plant stress: The case of ozone exposure. *Sensors* **2008**, *8*, 1740–1754. [CrossRef] [PubMed]
44. Förster, B.; Pogson, B.J.; Osmond, C.B. Lutein from deepoxidation of lutein epoxide replaces zeaxanthin to sustain an enhanced capacity for nonphotochemical chlorophyll fluorescence quenching in avocado shade leaves in the dark. *Plant Physiol.* **2011**, *156*, 393–403. [CrossRef] [PubMed]
45. Meroni, M.; Rossini, M.; Guanter, L.; Alonso, L.; Rascher, U.; Colombo, R.; Moreno, J. Remote sensing of solar-induced chlorophyll fluorescence: Review of methods and applications. *Remote Sens. Environ.* **2009**, *113*, 2037–2051. [CrossRef]
46. Wingler, A.; Lea, P.J.; Quick, W.P.; Leegood, R.C. Photorespiration: Metabolic pathways and their role in stress protection. *Philos. Trans. R. Soc. Lond.* **2000**, *355*, 1517–1529. [CrossRef] [PubMed]
47. Garbulsky, M.F.; Peñuelas, J.; Gamon, J.; Inoue, Y.; Filella, I. The photochemical reflectance index (PRI) and the remote sensing of leaf, canopy and ecosystem radiation use efficiencies: A review and meta-analysis. *Remote Sens. Environ.* **2011**, *115*, 281–297. [CrossRef]
48. Filella, I.; Porcar-Castell, A.; Munné-Bosch, S.; Bäck, J.; Garbulsky, M.; Peñuelas, J. PRI assessment of long-term changes in carotenoids/chlorophyll ratio and short-term changes in de-epoxidation state of the xanthophyll cycle. *Int. J. Remote Sens.* **2009**, *30*, 4443–4455. [CrossRef]
49. Kolber, Z. Laser Induced Fluorescence Transient (LIFT) Method for Measuring Photosynthetic Performance and Primary Productivity in Terrestrial Ecosystems. In Proceedings of the Earth Science Technology Conference, Pasadena, CA, USA, 11–13 June 2002.
50. Osmond, B. Understanding something that is remotely sensible, scaling active chlorophyll fluorescence from leaves to canopies at ranges of ~50 metres. *Tree Physiol.* **2014**, *34*, 671–673. [CrossRef] [PubMed]
51. Van der Tol, C.; Verhoef, W.; Timmermans, J.; Verhoef, A.; Su, Z. An integrated model of soil-canopy spectral radiances, photosynthesis, fluorescence, temperature and energy balance. *Biogeosciences* **2009**, *6*, 3109–3129. [CrossRef]
52. Gastellu-Etchegorry, J.P.; Lauret, N.; Yin, T.; Landier, L.; Kallel, A.; Malenovský, Z.; Al Bitar, A.; Aval, J.; Benhmida, S.; Qi, J.; et al. Recent advances in remote sensing data modeling with atmosphere, polarization, and chlorophyll fluorescence. *IEEE J. Sel. Top. Appl. Earth Obs. Remote Sens.* **2017**, in press. [CrossRef]
53. Fournier, A.; Daumard, F.; Champagne, S.; Ounis, A.; Goulas, Y.; Moya, I. Effect of canopy structure on sun-induced chlorophyll fluorescence. *ISPRS J. Photogramm. Remote Sens.* **2012**, *68*, 112–120. [CrossRef]
54. Pinto, F.; Müller-Linow, M.; Schickling, A.; Cendrero-Mateo, M.; Ballvora, A.; Rascher, U. Multiangular Observation of Canopy Sun-Induced Chlorophyll Fluorescence by Combining Imaging Spectroscopy and Stereoscopy. *Remote Sens.* **2017**, *9*, 415. [CrossRef]